Journal of
Marine Science and Engineering

MDPI

Article

Experimental Assessment of Planing Hulls Added Resistance in Regular Waves

Fabio De Luca, Claudio Pensa and Riccardo Pigazzini *

Dipartimento di Ingegneria Industriale, Università degli Studi di Napoli, 80125 Napoli, Italy
* Correspondence: riccardovasco.pigazzini@unina.it

Abstract: Amid a global effort in reducing the shipping ecologic impact, the study of the particular case of added resistance of high speed vessels cruising in a seaway has been approached by a very limited number of authors. In this study, we provide a comprehensive and systematic assessment of the added resistance of a planing hull in regular waves. The data are analyzed in both the time and frequency domains in order to fully characterize the added resistance and highlight its correlation with hull motions. It is found that peak added resistance modulation occurs for shorter waves with respect to the peak average added resistance, and slenderness is beneficial only in terms of modulation. Nonlinearity of both the average and first harmonic amplitude is also shown. In addition, results of the phase analysis show a correlation between the added resistance phase and average added resistance.

Keywords: systematic series; planing; added resistance

Citation: De Luca, F.; Pensa, C.; Pigazzini, R. Experimental Assessment of Planing Hulls Added Resistance in Regular Waves. *J. Mar. Sci. Eng.* **2023**, *11*, 141. https://doi.org/10.3390/jmse11010141

Academic Editor: Kostas Belibassakis

Received: 30 November 2022
Revised: 19 December 2022
Accepted: 22 December 2022
Published: 7 January 2023

1. Introduction

Today, although the International Maritime Organization already deploys policies frameworks in order to reduce [1] shipping greenhouse gas emissions, numerous energy-saving devices have been experimented with in order to reduce total hull resistance, but no particular guidelines are given to small fast crafts. Increased consumption, hull motions and resistance when operating any craft in waves are phenomena that are regularly evaluated when taking operational decisions on commercial routes in order to minimize those effects (weather routing). High-speed vessels are especially vulnerable to the effects of rough seas given their higher operational speed. In order to gain further insight in the phenomena related to the added resistance in waves, a systematic approach to the problem is needed in order to highlight the effects of both the hull shape, speed and wave parameters on added resistance. This can allow to have a better insight of the dynamics that govern the added resistance of planing hulls in waves.

Since very few studies have carried out such efforts, especially using an experimental approach, in this work, we study the effect of wave and hull characteristics on the added resistance of a subset of the Naples Systematic Series (NSS) hulls in regular waves. The main motive behind such a study lies in the desire to characterize a problem of known complexity, such as hull–wave interaction in high speed crafts, where stronger non-linear effects can be relevant [2–6].

One of the first systematic studies on the resistance of planing hulls in regular waves was provided by Fridsma in the late 1960s [2]. In his study, added resistance was reported, showing its trend, with respect to wave height at different wave heights.

Zarnick and Turner [7] studied the effect of an irregular seaway on motions and added the resistance of a very high length-to-breadth (L/B) planing hull.

Blok and Beukelman [8] provided results for a hull (heave, relative motion, vertical acceleration and added resistance) for a slender hull form with L/B = 8.

Grigoropoulos [9] studied the seakeeping performance of NTUA double-chine series hull forms in regular waves and reported also the added resistance response amplitude operators.

Regarding the Naples Systematic Series, Tavakoli et al. [10] reported some results for a limited set of tests on the C1 model in their work on the comparison between numerical (2D + t), experimental and CFD methods for the assessment of the dynamics of a planing hull in waves.

Bi et al. [11] also showed the average resistance in regular sea of the USV01 hull. They compared the motion response amplitude operators and resistance results from RANSE simulations with experimental data.

In the case of fast planing crafts, experiments showed that a linear system assumption is less appropriate, as hull dynamics is dominated by a combination of strongly nonlinear hydrodynamic phenomena that results in the pressures acting on the hull bottom.

Moreover, small hull attitude changes usually result in a significant change in the waterplane and total wetted area due to the typical planing hull V sections and chines. Those sudden changes will affect both induced pressures and added mass, as well as damping and restoring terms due to the large motions when cruising in a seaway, resulting in the nonlinear trends of both motion responses and added resistance. As the wave height increases along with hull motions, a large and sudden variation of the waterplane area in the bow sections can result in bow flare impacts, impulsive pressure peaks that introduce further nonlinearities in the hull dynamics forcing terms. Non-linear trends of the added resistance measured during regular waves tests can be classified based on the signal harmonic content, namely, first and second harmonic nonlinearities [12].

The scope of the present work is to extend the results shown in the previous study [12], characterizing added resistance in regular waves of a Naples Systematic Series (NSS) subset. In particular, the study focuses on the experimental data of C1s and C2s hulls. Added resistance data analyzed both in the time and frequency domains are presented in comprehensive plots highlighting the effects of both wavelength and wave steepness, as well as hull speed and slenderness ratio. Added resistance data will be presented in terms of average value, first-harmonic amplitude and phase difference with respect to the incoming wave. The frequency domain data analysis algorithm are based on the same principles used in the previous study [12] on regular waves seakeeping of the same hulls and speed combinations. The goal of the comprehensive set of experimental data analyzed and discussed in the present paper is to gain a better insight into the physical phenomena that lies behind the added resistance of planing hulls in waves, in particular, how the added resistance characteristics relate to other seakeeping parameters, such as vertical motions and accelerations and details about the phase changes with respect to incoming waves.

The data showed in this paper also represent a significant addition to the already published and well-studied NSS dataset with regular wave added resistance data, increasing its relevance in the research sector. The results presented in this work can be used as a first guess for the evaluation of added cyclic loads on high-speed craft power plants and propeller shafts, considering that also mild sea conditions can impact the propulsion system of planing hulls, as discussed in [13].

2. Experimental Setup

In this study, we used the C1s and C2s models of the Naples Systematic Series (NSS) [14]. These models have been built as a reduced scale of the main C1 and C2 models [14] in order to fit into the seakeeping test instrumentation limits. Sections and buttock lines of the parent model (C1) are shown in Figure 1 for reference. The C1s and C2s models were tested in the Università degli Studi di Napoli "Federico II" Towing Tank at the Department of Industrial Engineering. The tank measurements are length of 136.0 m, width of 9.0 m and depth of 4.5 m, the carriage maximum speed is 10.0 m/s. For the sake of consistency, the same mass configuration used in [12,15] was adopted, see Table 1.

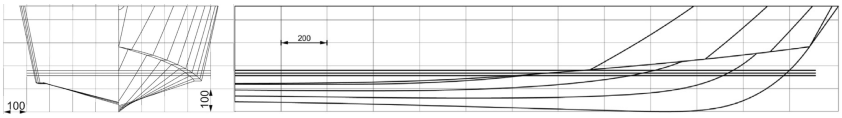

Figure 1. NSS parent hull body plan and buttock lines.

Table 1. Hulls specifications.

Model	C1s	C2s
L_{OA} (m)	1.567	1.567
L_{WL} (m)	1.44	1.44
B_{WL} (m)	0.446	0.396
LCG (m)	0.567	0.567
Δ (kg)	26.52	20.91
∇	4.83	5.23
A_T/A_X	0.94	0.94
L_{WL}/B_{WL}	3.23	3.64
B_{WL}/T	4.12	4.12
VCG/B_{WL}	0.5	0.5
K_{44}/B_{WL}	0.4	0.4
K_{55}/L_{WL}	0.25	0.25
β_T (deg)	13.2	13.2
$\beta_{0.5}$ (deg)	22.3	22.3
$\beta_{0.75}$ (deg)	38.5	38.5

The models were towed at 3.5 and 4.5 m/s, corresponding to $Fr = 0.93$ and $Fr = 1.20$ ($Fr_\nabla = 2.05$ to 2.74). Regular waves were generated using a flap wavemaker at the end of the towing tank. The range of tested wave frequency is from 0.40 to 1.0 Hz, wave steepness from $H/\lambda = 1/100$ to $H/\lambda = 1/20$. Due to time and instrumentation limits, not all combinations have been tested. The experimental matrices in Figure 2 show the measured wave frequency and steepness of all the cases tested in this study. C1s and C2s hulls differ from each other only by their L_{WL}/B_{WL} ratio (C2 is 11% slimmer), so differences in non-dimensional added resistance between the two hulls can be attributed to the effects of the slenderness ratio.

In order to provide a common case between the four hull–speed combinations, the ITTC recommended $H/\lambda = 1/50$ wave steepness was used as a reference when assessing speed and hull geometry effects.

AKAMINA AWP-24-2 wave height gauges capacitive probes and Baumer UNDK 30U6103 ultrasonic probes have been employed to sample the wave profile. The reference measurements for wave height are from the stationary capacitive probes , where the measurements from the ultrasonic probes fastened to the towing carriage were used for determining encounter wave frequencies and phase difference between wave and added resistance, particularly the one placed at the same longitudinal coordinate of the hull's CG. The calibrated capacitive probes were also used to check the wave-maker transfer functions in order to minimize the difference between nominal and effective wave characteristics. Hull motions (heave and pitch, in particular) have been captured using the Qualisys Motion Capture System, linked to the towing carriage. Accelerations were measured both at the center of mass CG and at the bow, 0.5 L_{WL} forward of center of gravity, using three-axis Crossbow CXL04GP3-R-AL MEMS accelerometers. The models were towed using a double-hinged shaft between the model and the towing arm (see Figure 3) through a HBM PW15AHC3 load cell (range: 0–20 kg, sensitivity: 2 g); yaw motion is constrained by the bow and aft vertical guides.

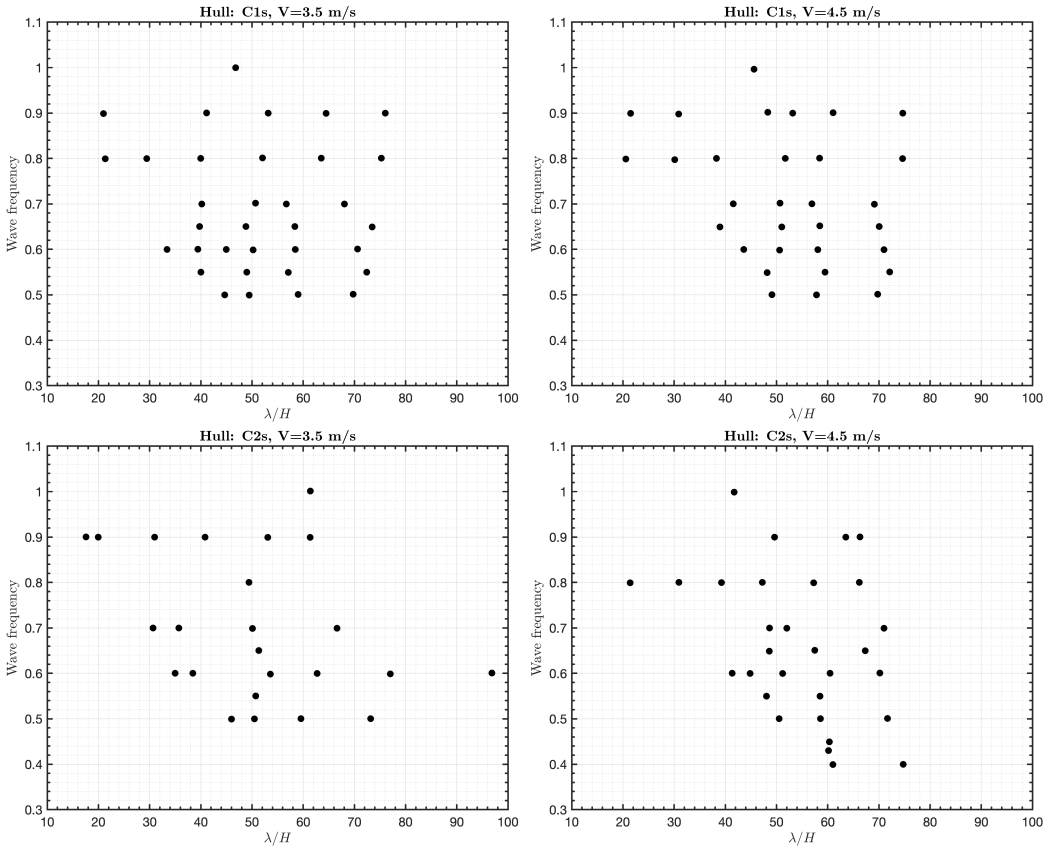

Figure 2. Experimental matrices of wave frequency and steepness for each hull and speed combination.

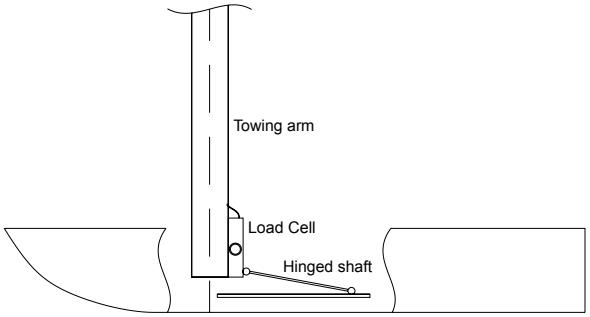

Figure 3. Experimental setup.

In Figure 4 a top view of both C1s and C2s is shown. The towing arm, load cell and hinged shaft are visible, as well as the bow and aft vertical guides. A spray guard was fitted to both models in order to avoid water ingress during some runs.

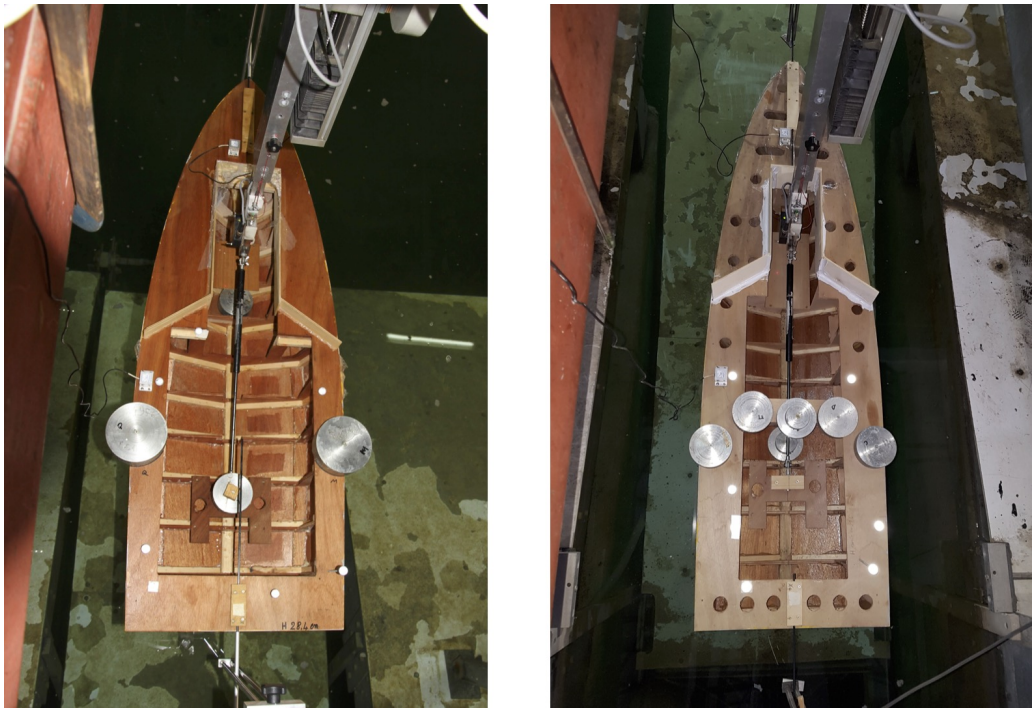

Figure 4. Top view of C1s (**left**) and C2s (**right**) hulls.

3. Results

In this section, average, amplitude and phase of the added resistance are discussed. First, the harmonic amplitude of the added resistance was obtained from the amplitude spectra of the original signal using FFT. The trend of the added resistance average value, first harmonic amplitude and phase is analyzed using both iso-steepness and iso-frequency plots. Figures of multiple charts in this section are presented so that the first row of plots refers to C1s hull plots and the second refers to C2s hull plots. The first column of charts is relative to the speed of 3.5 m/s and the second is relative to the speed of 4.5 m/s.

3.1. Average Response

The iso-steepness plots in Figure 5 show the average values of the non-dimensional added resistance vs λ/L_{WL}. The most obvious results from the plots in Figure 5 is that there is a common wavelength for which the average added resistance is maximal across different wave steepnesses/heights. In particular, looking at the plots corresponding to the same hull speed (column), the slenderness ratio seems to be not relevant in terms of the wavelength of the peak added resistance. The independence of hull geometry on the peak added resistance wavelength was also reported by Fridsma [2]; in his case, deadrise is mentioned. Looking at the plots corresponding to the same hulls (row) instead, it is clear how hull speed influences the peak added resistance wavelength, as it is around $\lambda/L_{WL} = 2.5$ for the lower speed, and at $\lambda/L_{WL} = 3.0$ for the higher speed. The fact that the wavelength at which the maximum added resistance is reached shifts with the hull speed was confirmed by other authors [2]. The shift in the peak wavelength is due to the fact that the same encounter/critical frequency is reached with longer waves when traveling at a higher speed. As expected, it can be clearly observed how increased speeds not only shift the peak wavelength, but also provide for higher values of added resistance.

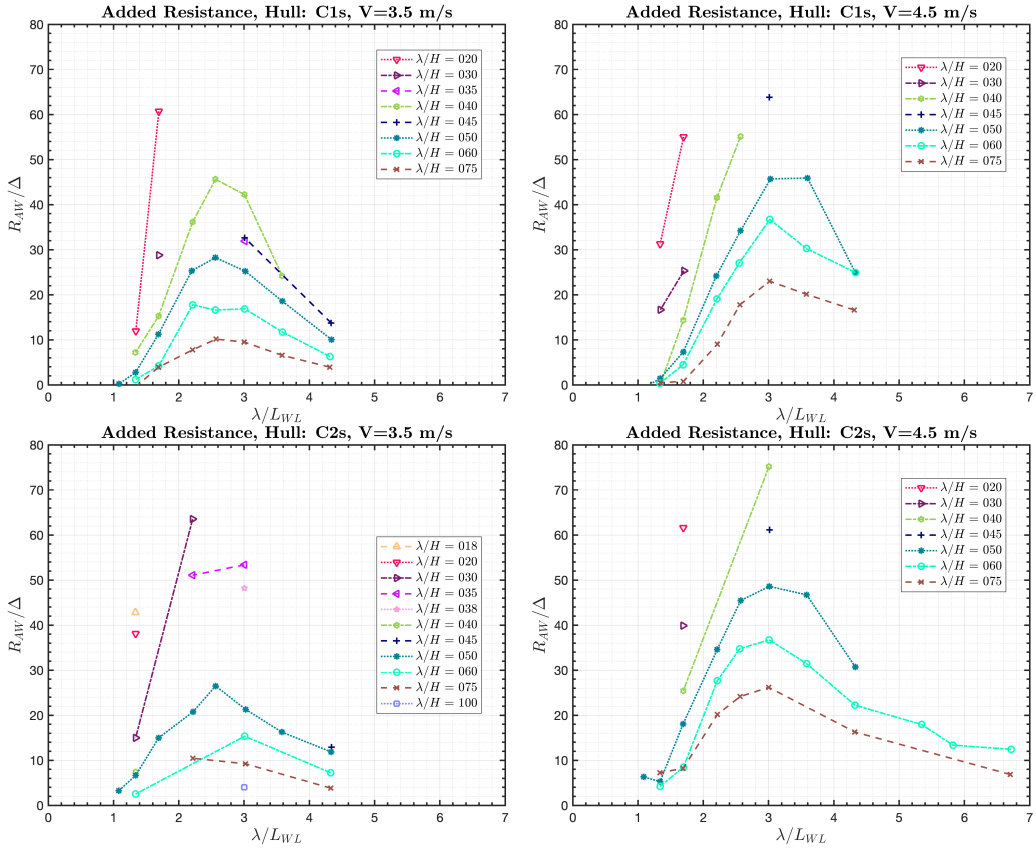

Figure 5. Added resistance vs. λ/L_{WL}.

Taking the $\lambda/H = 50$ case into consideration, a clear increase in peak added resistance with increasing speed is observed. An 18% increase in hull speed lead to an increase of around 70% in peak added resistance for the broader hull (C1s) and around 80% for the slimmer one (C2s).

Taking into account also a specific wavelength ratio of $\lambda/L_{WL} = 3.0$, non-dimensional added resistance increases by 88 and 118% respectively. The $\lambda/L_{WL} = 3.0$ represents the worst-case scenario, as it corresponds to peak added resistance values for the highest speed, but not for the lower one.

It is interesting to note that the the general trend of added resistance and bow acceleration (Figure 6) share some similarities, and both exhibit very similar, if not the same, peak wavelength and shift due to speed. This is not the case if the added resistance is compared to heave transfer functions (Figure 7), as the trends are very different with no substantial shift toward longer wavelengths with increasing hull speed being observed for heave.

In addition, as reported in [2], it is observed that maximum added resistance occurs at a shorter wavelength with respect to maximum hull motions.

Those observations could suggest that the average added resistance in the waves of a planing hull in regular waves has a stronger correlation with bow accelerations with respect to heave and pitch.

This can be expected, as higher acceleration response at the bow is due to stronger bow–wave impacts. As the hull's bow surfaces are more vertical, the pressures due to bow impacts have a higher horizontal component, contributing to increasing total resistance.

The iso-frequency plots in Figure 8 show the average values of the nondimensional added resistance vs. λ/H. As reported in earlier studies, the plots show quite clearly that given a constant wavelength, the added resistance is strongly dependent on wave height. Moreover, the dependency is nonlinear, and the added resistance seems to be proportional to some power of the wave height.

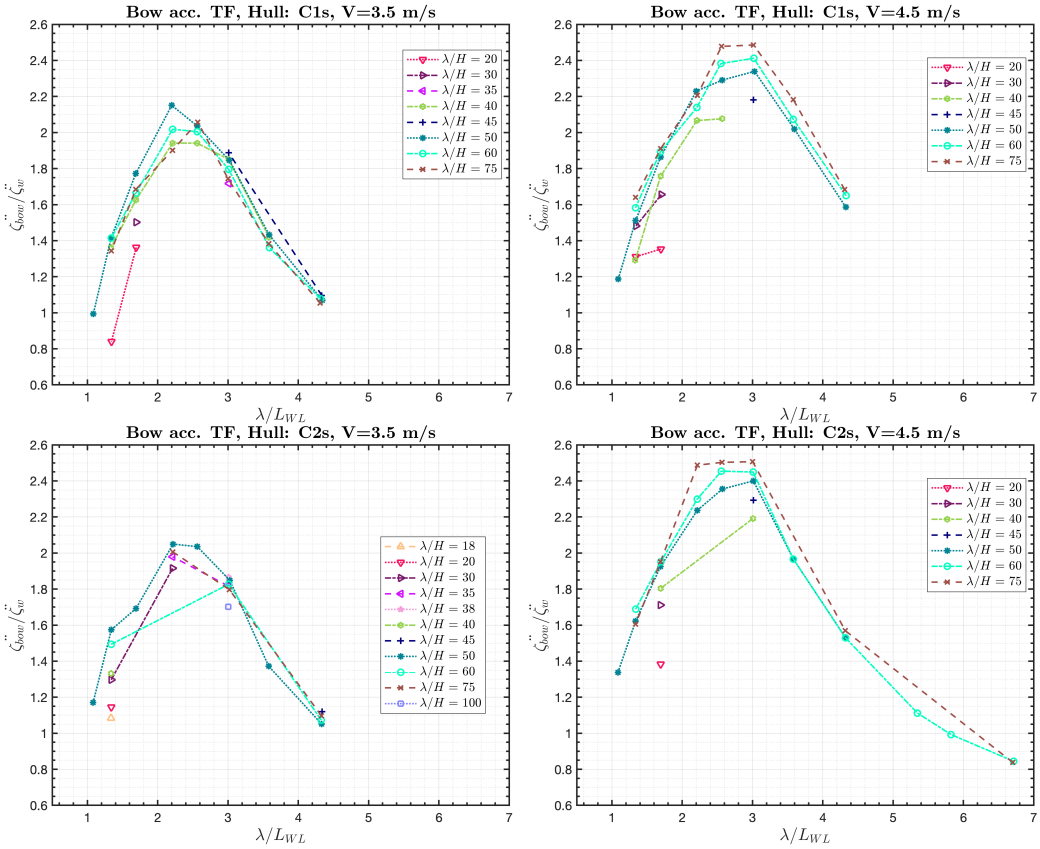

Figure 6. Vertical bow acceleration transfer functions vs. λ/L_{WL}.

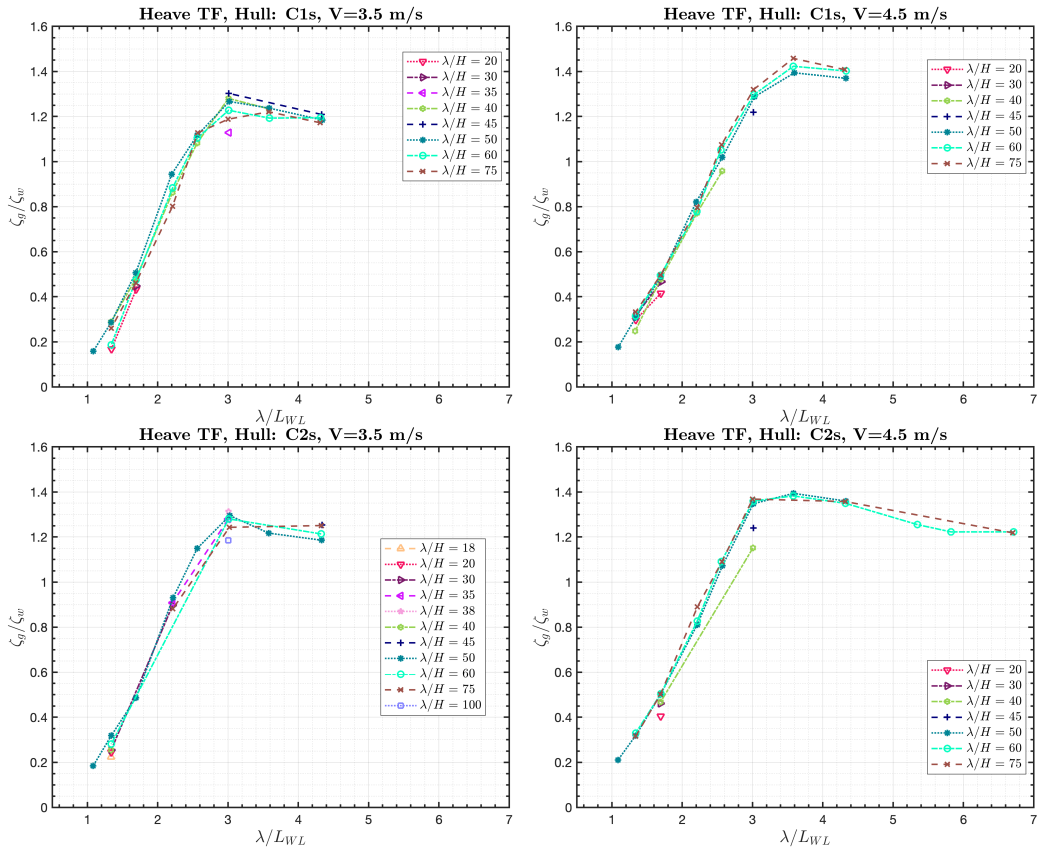

Figure 7. Heave response vs. λ/L_{WL}.

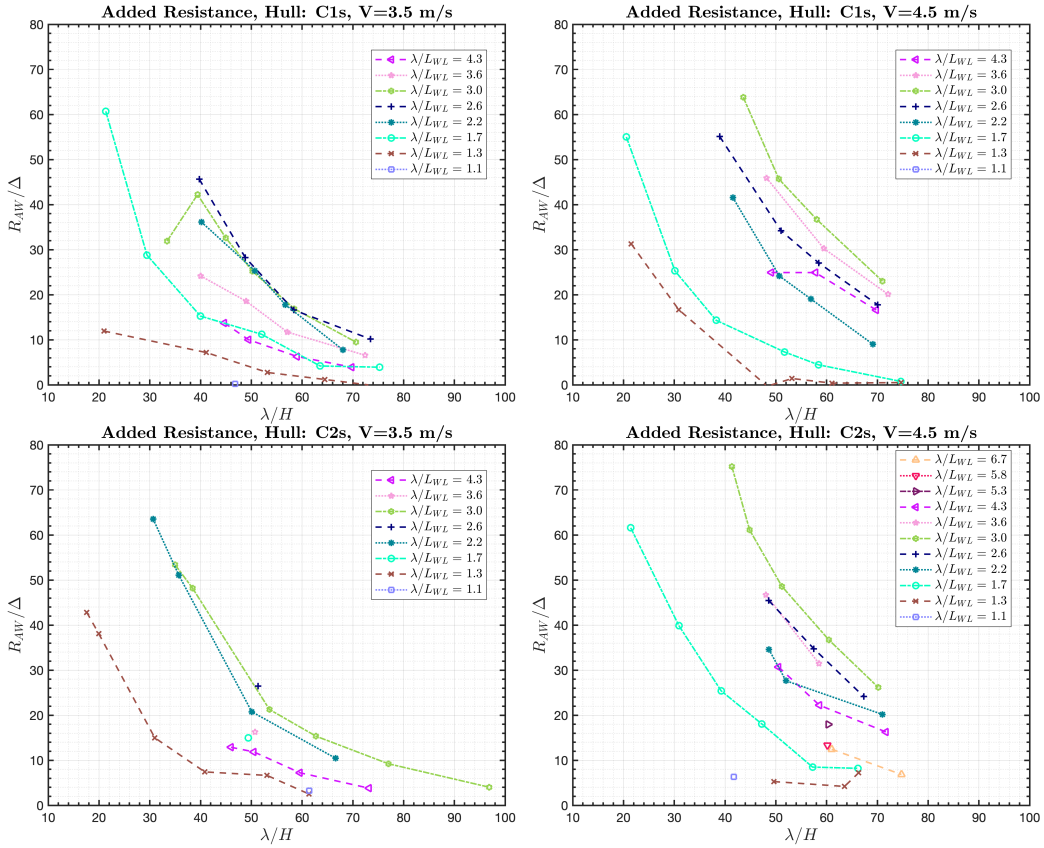

Figure 8. Added resistance vs. λ/H.

3.2. First Harmonic Response

In terms of hull performance, average values of the added resistance reported in the first subsection are enough to evaluate different designs. However, as in the case of motions, added resistance is a variable quantity, and its amplitude and frequency are modulated by the incident waves and hull motions. In order to gain further insight into the added resistance modulation characteristics, in this section, the analysis of the first harmonic amplitude of the added resistance is presented. The results complement the average values data of the previous section and will be useful for the understanding of the correlations between the forcing term (waves and motions) and the resulting added resistance. The data representation method remains the same as the previous figures and the one already used for the in-depth motions analysis in [12].

The iso-steepness plots in Figure 9 show the nondimensional amplitude of the first harmonic of the added resistance vs. λ/L_{WL}. In these plots, the presence of added resistance nonlinearities is evidenced by the vertical separation between the curves.

The results of the frequency domain analysis show that also the first harmonic amplitude of the added resistance (Figure 9) shows a peak value at a certain encounter frequency. Differently from the case of average added resistance (Figure 5), the peak wavelength for the first-harmonic amplitude of the added resistance appears not to be influenced by the hull speed. In fact, both hulls at both speeds have a peak response around $\lambda/L_{WL} = 2.2$.

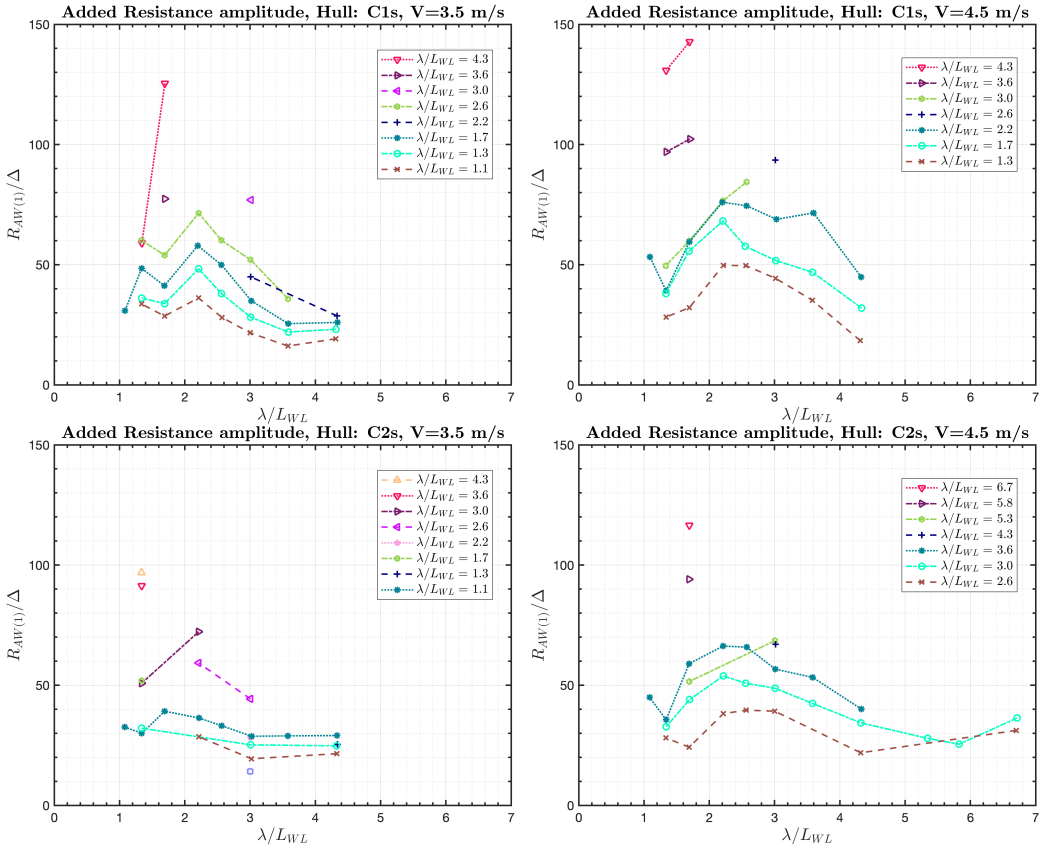

Figure 9. Added resistance first harmonic amplitude vs. λ/L_{WL}.

In terms of the added resistance amplitude, taking the $\lambda/H = 50$ case into consideration, both hulls show an increase in the added resistance modulation amplitude with increasing hull speed. In the case of the C1s hull, the increase (percentage) is half of what it is observed for the C2s hull (around 60% increase), and the same trend is also observed in the case of the average added resistance. Moreover, it can be observed that in this case, the slimmer the hull, the less the added resistance amplitude. The fact that there is no shift in the peak wavelength with speed means that when the speed is increased, both the amplitude and frequency of added resistance peak increase. Comparing the results shown in Figure 9 with the ones in Figure 5, we can see how peak added resistance modulation occurs at shorter wavelengths with respect to peak average values, particularly for higher speeds.

The iso-frequency plots in Figure 10 show the nondimensional amplitude of the first harmonic of the added resistance vs. λ/H.

The nonlinearity associated with added resistance modulation in regular waves are well-described in the iso-frequency plots. It can be observed that the amplitude of the added resistance also has a polynomial relationship with the wave height, and the higher the speed, the steeper it is, as it as the case with average values (Figure 8).

In Figure 11, the right plot shows the comparison between the frequency response of both signals. It is indeed clear that both share the same main peak frequency, but, for the case of the added resistance, a significant second harmonic is present.

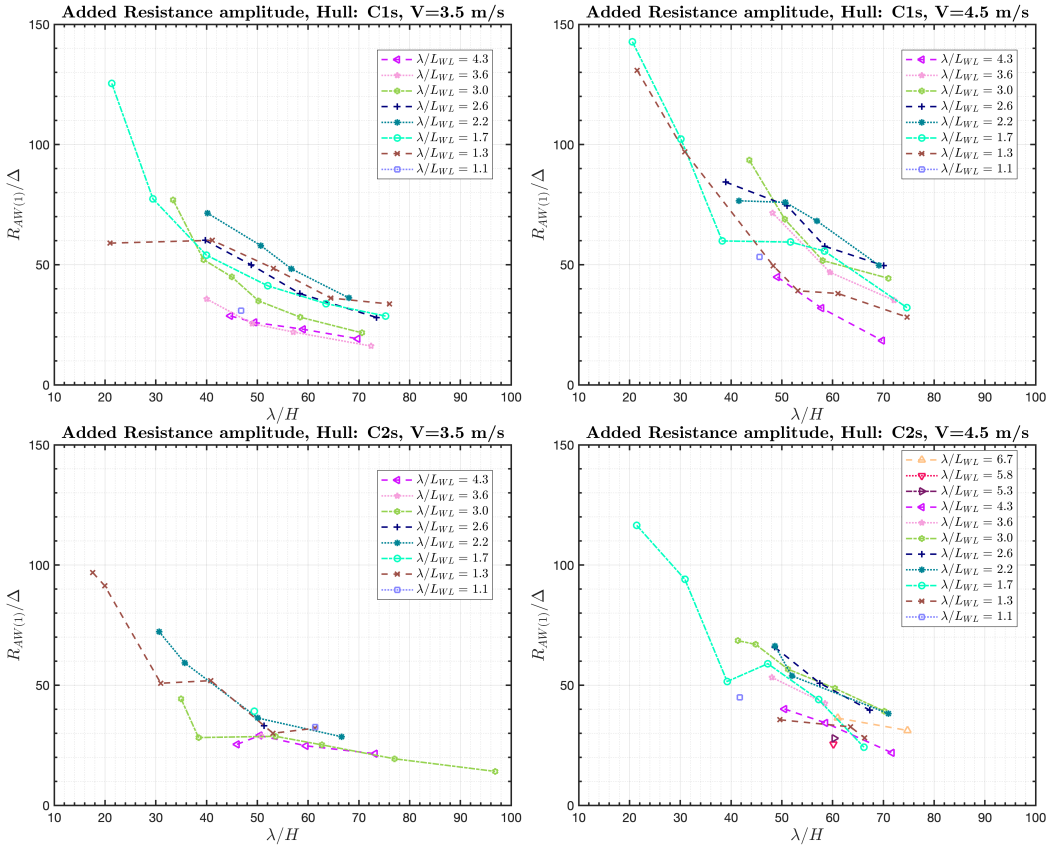

Figure 10. Added resistance first harmonic amplitude vs. λ/H.

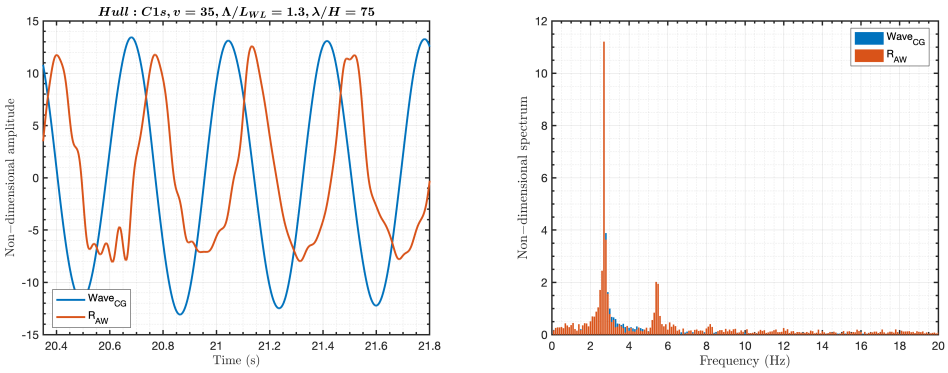

Figure 11. Example of added resistance time series and spectra.

Added resistance nonlinear behavior is expected, as the hull pitches down toward an incoming wave and the bow sub vertical hull surfaces impact with the wave slope, large horizontal forces are suddenly generated (around t = 20.7 s on the left plot). The vertical hydrodynamic and restoring forces then counteract the pitching inertia and lifts the bow over the water leading to lower added resistance values until the next bow impact (t = 20.8–21 s). The sudden increase in added resistance occurs over a shorter time span with respect to the period of lower added resistance, and the peaks are higher amplitude than troughs. This occurs as the hull motion resulting from the impact allows the sub vertical surfaces to be over the water until the next bow impact, allowing for a longer period of lower resistance.

3.3. Phase Response

In order to gain further insight into the principles that are governing the added resistance modulation, a detailed analysis of the phase of the added resistance respect to the incident waves was carried out and will be discussed in this section.

The evaluation of the added resistance phase was possible through the use of the wave elevation measurements at the longitudinal coordinate as the hull center of gravity. This dedicated wave elevation signal at CG was used as the reference signal. The added resistance phase was defined as the phase difference between the added resistance and wave elevation Φ_{AddRes}. In Figure 11, an example of the time series of added resistance and wave elevation with short waves shows the added resistance phase lead (i.e., added resistance peak at 20.4 s leads wave peak at 20.7 s).

In the following plots, added resistance phase is computed using the phase difference between the first harmonics of the added resistance and wave elevation signal by the use of a FFT-based algorithm. Given that, a decrease in phase difference means that the added resistance phase lead decreases. Also in the following plots, the results are presented using the same iso-steepness and iso-frequency plots approach used in the previous figures.

Looking at the iso-steepness plots in Figure 12, it can be observed that added resistance phases of both hulls at both speeds share a common trend (apart from the case of the C1s Hull at $v = 4.5$ m/s for long waves, discussed later) and the phase difference remains always positive. This means that the peaks of variable horizontal hydrodynamic forces constituting hull resistance modulation in waves are always leading the wave elevation at LCG (or wave elevation lags added resistance). This is expected, as most of the horizontal forces contributing to the added resistance originate from the bow sections interacting with the waves (for example, at the maximum wave slope), which will occur always earlier than when the hull's LCG reaches the same wave spot.

One of the most interesting aspects of the phase results is that there is a critical wavelength in which the added resistance phase lead is minimal. In this case, as it is for the first harmonic amplitude, a significant peak wavelength shift is not observed as in the case of average added resistance (Figure 5). The wavelength for minimal added resistance phase is around $\lambda/L_{WL} = 3.0$ for all four hull–speed combinations. Looking at the $\lambda/H = 50$ cases, the hull slenderness seems not to influence the minimum phase lead values.

When the added resistance phase plots in Figure 12 are compared with average added resistance in Figure 5, it can be observed that peak average added resistance occurs at a wavelength close to the minimum phase lead. When phases are compared instead with first harmonic amplitudes in Figure 9, it shows that the maximum resistance modulation amplitude occurs at a shorter wavelength with respect to the minimum added resistance lead. So, the increasing average added resistance appears to be better related with the decreasing added resistance phase lead than the actual resistance modulation amplitude.

Taking the $\lambda/H = 50$ cases, it can be noted that added resistance phase lead clearly decreases at the shortest wavelengths ($\lambda/L_{WL} = 1.3$–1.5) with increasing hull speed. Given the very limited hull motions in this conditions (see Figures 7 and 13), the decrease in phase lead cannot be due to different hull dynamics, but hull attitude changes (average pitch) instead. Since between 3.5 m/s and 4.5 m/s, the average hull pitch (trim) increases, waves hit the hull further aft at 4.5 m/s than at 3.5 m/s, thus reducing added resistance phase lead.

The iso-frequency plots in Figure 14 show that there is no clear trend in the added resistance phase with respect to wave steepness/height. This means that the main contribution toward the difference between the added resistance and wave phase is due more to the wavelength and hull speed than wave height. Moreover, the nonlinear effects seen in the average added resistance and its first harmonic amplitude do not affect the phase response.

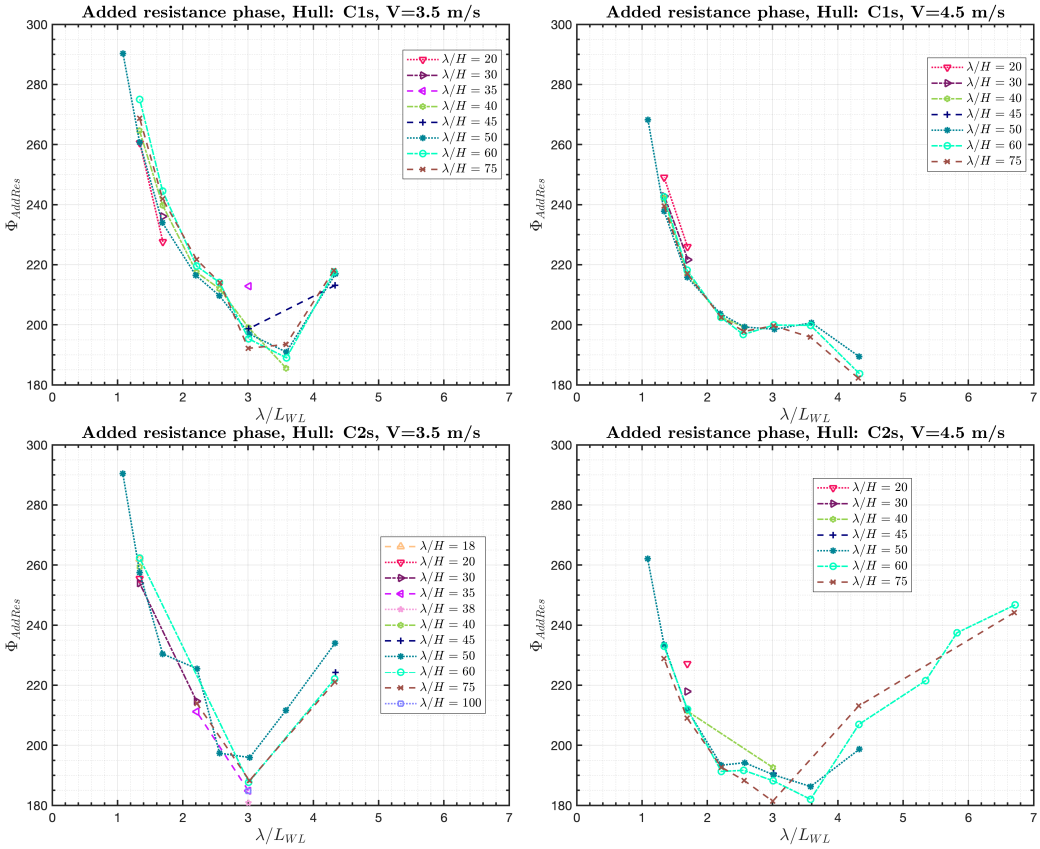

Figure 12. Added resistance phase vs. λ/L_{WL}.

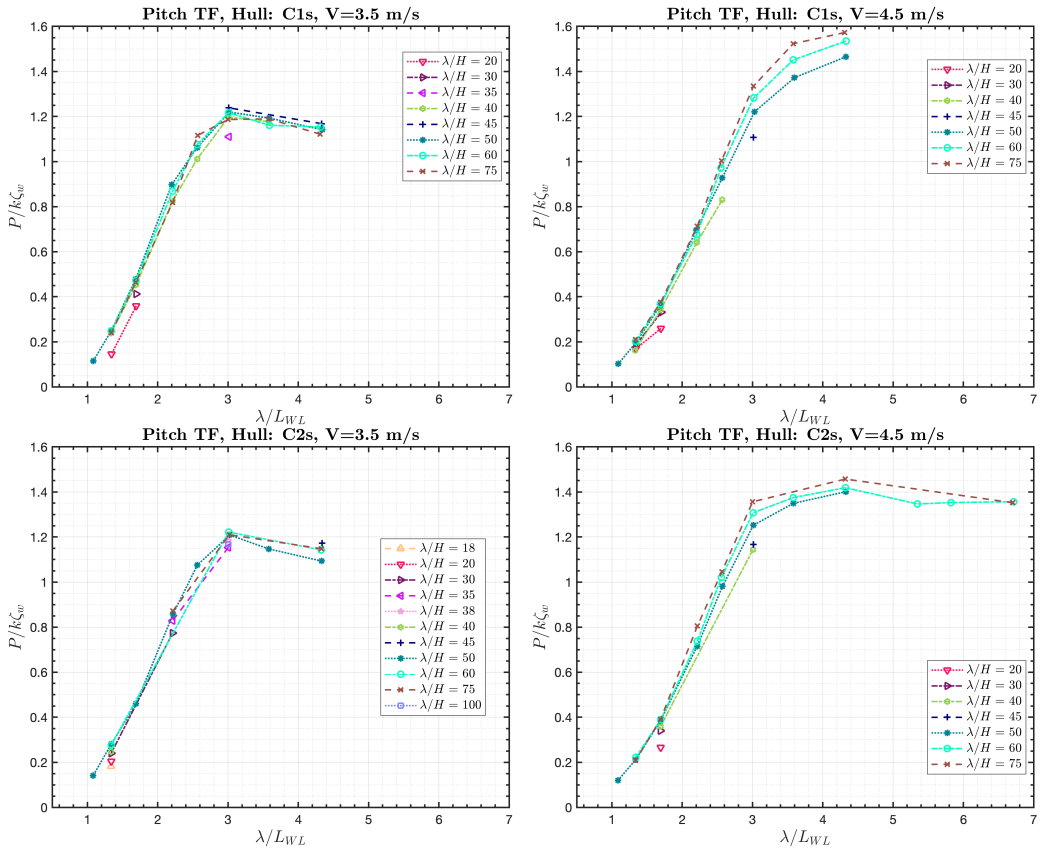

Figure 13. Pitch response vs. λ/L_{WL}.

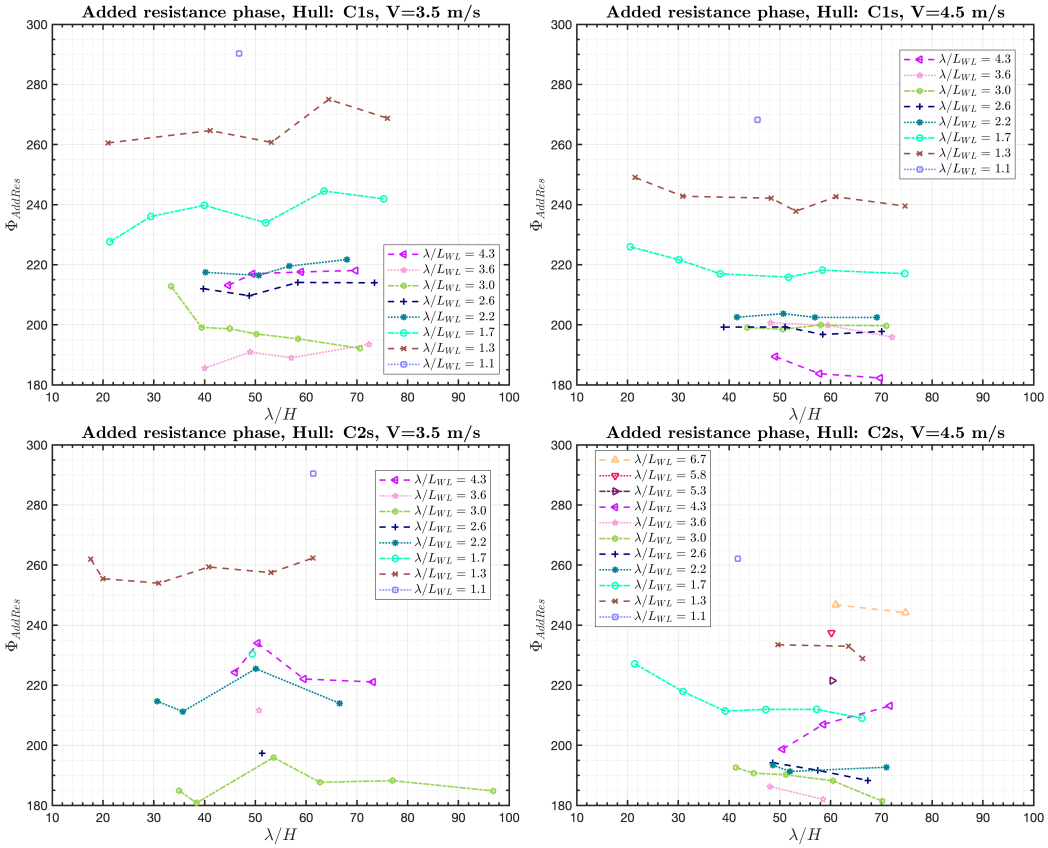

Figure 14. Added resistance phase vs. λ/H.

4. Conclusions

The present work showed a comprehensive experimental characterization of the added resistance in regular waves of hulls C1s and C2s from the Naples Systematic Series (NSS) for two hull speeds, both in the planing regime ($Fr_\nabla > 2.0$). The measured added resistance data were analyzed in both the time (average) and frequency (first harmonic and phase) domains in order to provide a detailed description of the phenomena. Results of the average added resistance, its first harmonic amplitudes and phase were shown both as iso-steepness and iso-frequency plots, highlighting the role of both the encounter frequency and wave steepness/height for each hull and speed combination.

Iso-steepness plots of average added resistance response showed that there is a specific wavelength ratio for which added resistance is maximal and it shifts toward higher values with increasing speed, but hull slenderness does not affect it. The comparison of the results with hull motions and accelerations suggests that average added resistance in regular waves is more correlated to bow accelerations than heave and pitch, hinting at the role of bow impacts on the added resistance of fast hulls.

Iso-frequency plots of average added resistance confirm what was observed also in previous studies, namely, the added resistance increases in a nonlinear fashion with wave height.

Iso-steepness plots of the first harmonic amplitude show that the added resistance modulation peaks at a specific wavelength ratio that does not depend on the hull or speed.

Considering modulation amplitudes, increasing the hull speed leads to higher amplitudes, whereas the hull slenderness has a beneficial effect, as the slimmer hull shows smaller added resistance oscillations. Comparing the first harmonic amplitude and average response results, it is observed that peak added resistance modulations occur for shorter waves with respect to the peak average added resistance.

Iso-frequency plots of the added resistance first harmonic amplitude show that there is a strong nonlinear dependency with wave steepness/height.

Added resistance phase with respect to the incident wave were also analyzed in order to provide a comprehensive picture of the added resistance phenomenon.

Iso-steepness plots of the added resistance phase show that for all speed–hull combinations, the phase is always positive and has a similar trend with wave frequency. The fact that added resistance always leads the wave elevation at LCG confirms that the horizontal forces underlying the phenomena are developed in the bow sections of the hull. The effect of hull attitude changes on the added resistance phase lead are also shown. Iso-frequency plots of the added resistance phase show that nonlinear effects are absent.

Phase analysis shows that there is a critical wavelength ratio in which added resistance phase lead is minimal, which is common between all four hull–speed configurations. It is interesting to note that also at the critical wavelength ratio, the peak average added resistance occurs, but the same is not valid for the peak added resistance modulation amplitude. These observations suggest that a decrease in the added resistance phase lead is correlated to increased average added resistance.

Future plans for the study of added resistance in regular sea include self-propulsion experiments as well as performing regular waves experiments with the C3, C4 and C5 hulls of the Naples Systematic Series.

Author Contributions: Conceptualization, F.D.L., R.P.; methodology, F.D.L., R.P.; software, F.D.L., R.P.; validation, F.D.L., R.P.; formal analysis, F.D.L., R.P.; investigation, F.D.L., R.P.; resources, F.D.L., R.P.; data curation, F.D.L., C.P., R.P.; writing—original draft preparation, F.D.L., C.P., R.P.; writing—review and editing, F.D.L., C.P., R.P.; visualization, F.D.L., C.P., R.P.; supervision, C.P.; project administration, C.P.; funding acquisition, C.P. All authors have read and agreed to the published version of the manuscript.

Funding: This research was partially funded by the PRIN 2017 program, project 2017X7Z8S3 "LUBRI-SMOOTH: Innovative materials and techniques for the reduction of ship resistance".

Institutional Review Board Statement: Not applicable.

Informed Consent Statement: Not applicable.

Data Availability Statement: Not applicable.

Acknowledgments: The PRIN 2017 program, project 2017X7Z8S3 "LUBRI-SMOOTH: Innovative materials and techniques for the reduction of ship resistance", is gratefully acknowledged for the financial support.

Conflicts of Interest: The authors declare no conflict of interest.

Nomenclature

The following symbols are used in this manuscript:

Symbol	Description	Symbol	Description
L_{OA}	Length Overall (m)	R_{AW}	Added resistance (kg)
L_{WL}	Waterline Length (m)	β_T	Deadrise at the transom (deg)
B_{WL}	Waterline Breadth (m)	$\beta_{0.5}$	Deadrise at 0.5 L_{WL} (deg)
LCG	Longitudinal Center of Gravity (m)	$\beta_{0.75}$	Deadrise at 0.75 L_{WL} (deg)
VCG	Vertical center of gravity (m)	λ	Wavelength (m)
Δ	Model Weight (kg)	H	Wave height (m)
v	Speed (m/s)	ω_e	Encounter angular frequency (s^{-1})
g	Acceleration of gravity (m/s^2)	H_n	Amplitude of n-th Heave amplitude harmonic (m)
A_T	Area of Transom (m^2)	P_n	Amplitude of n-th Pitch amplitude harmonic (m)
A_X	Area of Maximum Transverse Section (m^2)	$\mathbb{M}$	Length-displacement ratio ($L_{WL}/\Delta^{1/3}$) $(-)$
T	Draught (m)	Fr	Froude Number ($v/\sqrt{gL_{WL}}$) $(-)$
K_{44}	Roll radius of gyration (m)	Fr_∇	Volumetric Froude Number ($v/\sqrt{g(\Delta/\rho)^{1/3}}$) $(-)$
K_{55}	Pitch radius of gyration (m)		

References

1. Marine Environment Protection Committee. *Resolution MEPC. 203 (62) Amendments to the Annex of the Protocol of 1997 to Amend the International Convention for the Prevention of Pollution from Ships, 1973, as Modified by the Protocol of 1978 Relating Thereto*; Technical Report; International Maritime Organization: London, UK, 2011.
2. Fridsma, G. *A Systematic Study of the Rough-Water Performance of Planing Boats*; Technical Report; Stevens Institute of Technology, Davidson Laboratory: Hoboken NJ, USA, 1969.
3. Van den Bosch, J. *Tests with Two Planing Boat Models in Waves*; Report No. 266; TU Delft, Faculty of Marine Technology, Ship Hydromechanics Laboratory: Delft, The Netherlands, 1970.
4. Masatoshi, B. Motions of a High Speed Planing Boat in Regular Head Sea. *Bull. Soc. Nav. Archit. Korea* **1977**, *14*, 36–44.
5. Chiu, F.c.; Fujino, M. Nonlinear prediction of vertical motions and wave loads of high-speed crafts in head sea. *Int. Shipbuild. Prog.* **1989**, *36*.
6. Tiao, W.C. Experimental investigation of nonlinearities of ship responses in head waves. *Appl. Ocean Res.* **2011**, *33*, 60–68.
7. Zarnick, E.E.; Turner, C. *Rough Water Performance of High Length to Beam Ratio Planing Boats*; Technical Report; David W Taylor Naval Ship Research and Development Center: Bethesda, MD, USA, 1981.
8. Blok, J.J.; Beukelman, W. The high-speed displacement ship systematic series hull forms–seakeeping characteristics. *Soc. Nav. Archit. Mar. Eng. Trans.* **1984**, *92*.
9. Grigoropoulos, G.; Damala, D.P.; Loukakis, T.A. Dynamic performance of the NTUA Double-Chine series hull forms in regular waves. In Proceedings of the 11th International Conference on Fast Sea Transportation FAST, Honolulu, HI, USA, 26–29 September 2010.
10. Tavakoli, S.; Bilandi, R.N.; Mancini, S.; De Luca, F.; Dashtimanesh, A. Dynamic of a planing hull in regular waves: Comparison of experimental, numerical and mathematical methods. *Ocean Eng.* **2020**, *217*, 107959.
11. Bi, X.; Zhuang, J.; Su, Y. Seakeeping Analysis of Planing Craft under Large Wave Height. *Water* **2020**, *12*, 1020.
12. Pigazzini, R.; De Luca, F.; Pensa, C. An experimental assessment of nonlinear effects of vertical motions of Naples systematic series planing hulls in regular waves. *Appl. Ocean Res.* **2021**, *111*, 102546. https://doi.org/10.1016/j.apor.2021.102546.
13. Pigazzini, R.; De Luca, F.; Balsamo, F.; Migali, A.; Vitiello, L. Full-scale propulsion measurements on a planing pleasure yacht in waves. *Ocean Eng.* **2022**, *254*, 111149.
14. De Luca, F.; Pensa, C. The Naples warped hard chine hulls systematic series. *Ocean Eng.* **2017**, *139*, 205–236.
15. De Luca, F.; Pensa, C. The Naples Systematic Series–Second part: Irregular waves, seakeeping in head sea. *Ocean Eng.* **2019**, *194*, 106620.